0191–8141(95)00100–X

Physical models of regional fold superposition: the role of competence contrast

M. K. JOHNS and S. MOSHER

Department of Geological Sciences, University of Texas at Austin, Austin, TX 78712, U.S.A.

Abstract—Physical models of superposed folds demonstrate that rheologic contrast strongly controls the style of fold interference. Rheologic contrast affects strain partitioning between layer-parallel shortening and buckling and affects the development of structural anisotropies parallel to first-generation folds. Laminates with insignificant competence contrast are characterized by circular to elliptical domes and basins (Type 1 interference). In addition to folding, the layers accommodate shortening by layer-parallel thickening, preferentially in the fold culminations. Laminates with significant competence contrast are characterized by buckled fold hingelines and axial surfaces (Type 2 interference). The less competent layers thicken in the hinges; the more competent layers maintain their initial thickness. In plan view, the F_1 hingelines are refolded in a lobate–cuspate to box style, whose axial traces form conjugate pairs.

The models are dynamically scaled to represent folds with km-scale wavelengths. The evolution of surface structures, map patterns at different depths, and equal-area projections synthesized from structure contour maps were used for analysis, comparable to regional analysis common to field studies. Gravitational body forces effectively damp the vertical amplitudes of both the first and second generation folds, thereby enhancing the formation of Type 2 interference.

INTRODUCTION

Fold interference patterns are used to identify areas of polyphase deformation and to evaluate their kinematic evolution. The geometry of fold superposition has been characterized as Type 1, 2 or 3, based on the angle between the first fold axial surface and the superposed displacements (Ramsay 1962, 1967, p. 521). Field analyses, theoretical analyses and computer simulations of interference patterns have concentrated on similar folds, the fold style characteristic of layering with little competence contrast (Ramsay 1962, 1967, p. 422, Thiessen & Means 1980, Thiessen 1986, Perrin *et al.* 1988, Watkinson & Thiessen 1988). Such interference patterns have been reproduced in card-deck experiments in which passive line markers were deformed by heterogeneous simple shear (O'Driscoll 1962, 1964) and in Plasticine models (Reynolds & Holmes 1954).

Folds are also superposed in rocks with mechanically active layering, where there is significant competence contrast and buckling is the important fold mechanism (Hudleston 1973, Julivert & Marcos 1973, Julivert 1986, Stewart 1987, Stauffer 1988, Fowler 1989, Schwerdtner & van Berkel 1991, Stewart 1993). The interference style of superposed buckle folds is distinct from that of superposed passive folds.

Geometrical analyses assuming deformation by isometric bending predict that a competent layer cannot refold as a simple dome or basin structure (Lisle *et al.* 1990). Instead, crenulations with axes oblique to the major fold trends, termed curvature-accommodation folds, are necessary to accommodate the polyphase buckling of a competent layer. The curvature-accommodation folds produce closed interference map patterns with multiple inflections of curvature. Stauffer (1988) has mapped such structures in the field.

Experimental studies have demonstrated that superposed buckling of single layers or of multilayers with high competence contrast produces distinctive structural styles, fold mechanisms and strain accommodation (Ghosh & Ramberg 1968, Ghosh 1974, Skjernaa 1975, Watkinson 1981, Dubey 1984, Raj 1984, Odonne & Vialon 1987, Ghosh *et al.* 1992, 1993, Grujic 1993), as recently summarized by Grujic (1993).

In our study, multilayers with either negligible or significant competence contrast were shortened sequentially in two orthogonal directions. The models were designed to compare the interference formed by non-coaxial, superposed folds that formed under the same boundary and deformation conditions, for materials of different rheologic contrasts. Unlike some previous experiments where the first generation folds were pre-formed (e.g. Watkinson 1981, Ghosh *et al.* 1992, 1993, Grujic 1993), in this study folds of both generations formed experimentally. In this manner, we test the effect of F_1 fold heterogeneities on F_2 style and contrast the fold styles of both generations. To test the effect of gravitational body forces on the structural style of both generations of folds, models were deformed in a centrifuge. Previous models of superposed buckle folds had gravitational body forces that were insignificant with respect to lateral surface forces and are thus comparable to natural folds with wavelengths less than about 200 m (Ramberg 1967, p. 75). In this study, physical models deformed in a centrifuge are analogs of km-scale fold interference. Accordingly, models were analyzed using methods common to the field geologist. Models were analyzed by comparing the models' surface structures

Table 1. Parameters used for scaling calculation (Experiment c217)

		Unit	Material	Model	Nature	Model/nature
Density	ρ	kg m^{-3}	DC	1.1 × 10³*	2.2 × 10³†	5.0 × 10⁻¹
			PL	1.9 × 10³*		
Eff. viscosity	η	Pa s	DC	1.0 × 10⁵‡	1.0 × 10¹⁹§	1.0 × 10⁻¹⁴
			PL	1.0 × 10⁷‡	1.0 × 10²¹‖	1.0 × 10⁻¹⁴
Strain rate	ε	s⁻¹		2.0 × 10⁻³*	1.0 × 10⁻¹⁴¶	2.0 × 10⁻¹¹
Accel.	g_{max}	m s⁻²		9.2 × 10³*	9.8	9.4 × 10²
	g_{mean}			5.2 × 10³*	9.8	5.4 × 10²
	g'			7.1 × 10³*	9.8	7.2 × 10²
Resistive force	$\tau = \varepsilon\eta$	Pa	DC	2.0 × 10²§	1.0 × 10⁵§	2.0 × 10³
			PL	2.0 × 10⁴§	1.0 × 10⁷§	2.0 × 10³
Body force	$\sigma = \rho gh$	Pa		§		2.0 × 10³
Length	$h = \sigma/\rho g$	km		1.0 × 10⁻⁵	2.4§	4.3 × 10⁻⁶ calc. from g_{max}
				1.0 × 10⁻⁵	1.3§	7.5 × 10⁻⁶ calc. from g_{mean}
				1.0 × 10⁻⁵	1.8§	5.5 × 10⁻⁶ calc. from g'

*Data measured in this study.
†Data from Turcotte & Schubert (1982).
‡Data from Weijermars & Schmeling (1986) and references therein.
§Data calculated from other parameters.
‖Marble at approx. 500°C, Data from Carter (1976).
¶Data from Pfiffner & Ramsay (1982).

Table 2. Centrifuge run time

Model No.	Time (min)			rpm$_{max}$	g_{max}
	D_1	D_2	Total		
c223	28.58	28.67	57.25	2000	940
c226	26.87	28.69	55.56	2000	940
c215	5.51	40.10	45.62	2000	940
c224	37.67	15.06	52.73	2000	940
c216	12.00	18.24	30.24	2000	940
c222	42.08	31.61	73.69	2000	940
c218	52.68	55.95	108.64	2000	940
c217	33.18	61.10	94.28	2000	940
c220	27.54	62.63	90.17	2000	940
c221	32.54	95.03	127.57	2000	940
c213	6.51	13.03	19.54	2000	940

and horizontal sections, representing map views, fold axial traces, structure contours and the orientation of layering and fold axes.

METHODS

Stratigraphy

Laminates with negligible competence contrast are represented by differently colored layers of a single material. Laminates were made of relatively incompetent silicone bouncing-putty (Dow Corning dilatant compound #3179, abbreviated hereafter as DC), relatively strong Harbutt's Plasticine modeling clay (PL), or a homogeneous mixture of equal parts of the two. Both the modeling clay and silicone putty are power-law visco-elastic materials, and the modeling clay has an effective viscosity approximately two orders of magnitude larger than that of the silicone putty under the present experimental conditions (Tables 1 and 2, Appendices A and B; McClay 1976, Dixon & Summers 1985, Weijermars 1986). Layers were stacked and rolled together. Although no strong rheologic contrast existed

between the layers, a layer-parallel, planar anisotropy may have been induced by rolling and by trapping air bubbles between the layers. The base of each model was a 1 mm layer of DC, which acted as a weak detachment layer, except where the laminate was itself entirely DC (models c223 and c226). The PL laminate (model c215) comprised 16 layers, with a total thickness of 4 mm. The laminates of DC or the DC–PL mixture comprised 12 layers, with a total thickness of 3 mm.

Laminates with significant competence contrast were represented by alternating layers of DC and PL. The layers were stacked and quickly rolled together to form multiple, uniform thickness layers, using the microlaminate technique described by Dixon & Summers (1985). Air bubbles trapped in stacking may have served as perturbations that initiated buckling. Each model comprised a 12 or 16 layer multilaminate of total thickness 3 mm, over a 1 mm DC basal detachment.

A square grid with 5 mm spacing and grid lines parallel to the shortening directions was printed (using the photocopier technique of Dixon & Summers 1985) on the top surface of all the models before deformation (Figs. 2–4). To reduce boundary effects, the base and vertical faces of all models were lubricated (National Wax Co., Paxwax 6364-1A) before deformation.

Deformation

Models were shortened in two orthogonal directions in a centrifuge, using a hydraulic ram (designed by M. P. A. Jackson) similar to that of Dixon & Summers (1985) (Fig. 1, Appendix A). Deformation in the centrifuge allows use of relatively viscous materials to represent regional-scale structures that are affected by both tectonic and gravitational forces. The known and estimated experimental parameters yield a ratio of lengths (model to nature) of approximately 5 × 10⁻⁶ (Appendix B, Table 1). For example, 1 cm length in the model is analogous to about 2 km in nature. Individual layers in
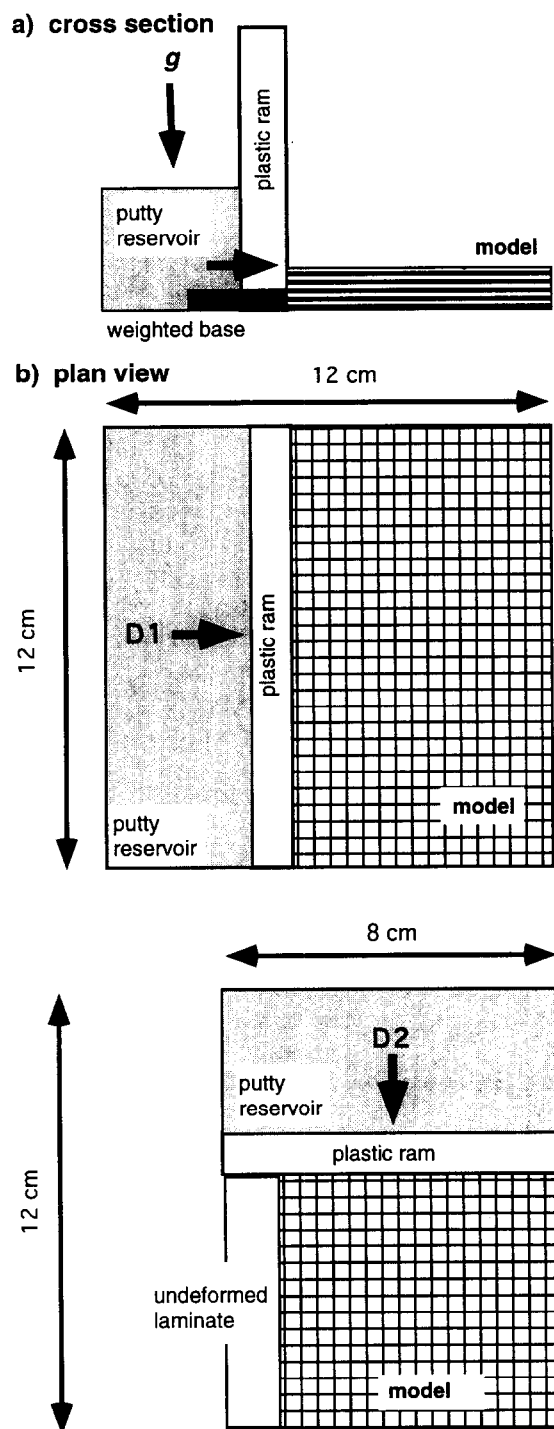
a) cross section

b) plan view

12 cm

8 cm

Fig. 1. Schematic set-up of deformation apparatus used in the centrifuge. For all models, layering is parallel to the centrifuge's equipotential surface. (a) The centrifuge's rotation axis is normal to the page. The centrifugal acceleration (g) causes dense putty to spread and displace a hydraulic ram. (b) The centrifuge's rotation axis is parallel to the page. After D_1, a strip of undeformed laminate was inserted to fill space in the centrifuge cavity. For plan views in the following figures, the D_2 shortening direction is oriented north.

the microlaminate are approximately 0.025 cm thick, analogous to strata 50 m thick in nature.

Analysis

Structural evolution was studied from photographs of the model surface taken after each time step of centrifu-

gal deformation. For select models, anticlinal hinges of the first generation folds were marked on the model surface after D_1 (heavy ink lines on model surfaces Figs. 2f, 4a & c) for comparison with the deformed F_1 hinges after D_2. After D_2 deformation was complete, the models were removed from the centrifuge, frozen and horizontally sectioned at 2 mm intervals. Profiles at the model boundaries were photographed for most models; however, no serial vertical sections were cut. Layer thicknesses were measured from the profiles. Because strain is most heterogeneous at the model boundaries, these measurements should be considered approximations. Crest-to-crest wavelengths of first (F_1) and second (F_2) generation folds were measured from plan-view photographs of the models' surfaces. The three-dimensional geometry of the structures was qualitatively evaluated by comparing horizontal sections from different depths and by comparing horizontal sections and profiles.

To analyze the fold geometry more quantitatively, structure contour maps and stereograms were constructed (cf. Skjernaa 1975). Layer contacts of select models were digitized from photographs taken at 2 mm depth intervals. The digitized data volume was gridded using a kriging algorithm and contoured for individual deformed surfaces with the software Spyglass Transform. Comparison of the contours, a reconstructed three-dimensional surface, the digitized layer contacts and photographs of the model surface confirm that the reconstruction technique accurately reproduces the major structural trends, but may smooth some of the minor folds. Strikes and dips were calculated from a finite difference estimation of the first derivatives in the grid directions. These slopes were plotted and contoured using the method of Kamb (1959) on lower hemisphere, equal-area projections representing the entire model or select domains. Trend and plunge of fold hinges were measured at even intervals directly from the structure contours.

RESULTS

Preliminary experiments

Several models were deformed in the centrifuge to test whether the basal and confining materials were appropriate (Appendix C). The results of the preliminary experiments confirmed the necessity of having a basal detachment layer, the appropriateness of using DC as a detachment material and the value of deforming the models with an unconfined upper surface.

Low competence contrast

Low competence contrast stratigraphy was deformed in five models (Table 3, Fig. 2). Models lacking a basal detachment are described in Appendix C. The rheologic contrast between the basal detachment and the laminate

controlled deformation, such that the laminate buckled as well as thickened. The rheology of the laminate controlled the differences in amplitude and wavelength between the PL laminates (Figs. 2a & b; c215) and the DC–PL mixtures (Figs. 2c & d; c216; Figs. 2e–g; c224) (Table 3). The degree of strain controlled differences between amplitude, wavelength and layer-parallel shortening of the two DC–PL mixture models (Figs. 2c–g; Table 3). After D_2, the high strain DC–PL laminate (c224) thickened by approximately 230%, whereas the moderate strain DC–PL laminate (c216) thickened by at least 160%.

For all three models, during the first phase of shortening (D_1) doubly plunging F_1 hinge-lines developed normal to the shortening direction and parallel to the ram. The F_1 axial surfaces are generally upright. Parasitic folds are present at the contact between the laminate and the DC detachment.

During D_2, regardless of rheology or degree of shortening, F_1 hingelines folded into domes and basins with upright, approximately planar F_1 and F_2 axial surfaces (cf. Ramsay 1962) (Fig. 2). In models with differential shortening (c215; Figs. 2a & b), domes and basins are elongate normal to the direction of greater shortening; they are equant for the model with approximately equal degrees of D_1 and D_2 shortening (c216; Figs. 2c & d). Horizontal sections show simple circular to elliptical interference patterns, which lack multiple inflections of curvature (Figs. 2b, d & g). Rare, crescent-shaped interference occurs where small domes or basins are juxtaposed (central region of c216; Fig. 2c).

Structure contours and poles to the top surface were reconstructed for model c216 (DC–PL mixture, D_1 = 36%, D_2 = 31%) (Figs. 5 and 6a). Data from transects on individual limbs and the crest of a major anticline yield the orientations of local F_1 axes and the combined data yield F_2 axes (Fig. 6b). The orientation of F_1 and F_2 hinges demonstrates that both F_1 and F_2 hingelines are curved, but lie on approximately planar, steeply dipping, orthogonal axial surfaces (Fig. 6c).

High competence contrast

Six models of alternating DC and PL layers demonstrate that buckle-fold interference is more complex where the stratigraphy has a high competence contrast (Table 4, Figs. 3 and 4).

The F_1 folds are typically doubly plunging (Fig. 3a). With progressive D_1 shortening, these periclines linked to form folds with apparently curved hingelines and axial surfaces, a process also observed in other buckle-fold models (Ghosh & Ramberg 1968, Blay et al. 1977, Dubey & Cobbold 1977, Guterman 1980). Folds in models with high competence contrast have shorter F_1 wavelengths for the same amount of shortening than F_1 wavelengths in low competence contrast models (Table 4). In profile, the F_1 fold styles are predominantly lobate–cuspate, but also include box style and chevron (Fig. 3a). The PL layers tend to maintain their thickness and commonly are fractured and rarely faulted in the

inner arc of anticlines. The DC layers are thickened in the hinges.

During D_2, F_1 hingelines and axial surfaces folded to produce both Type 1 and Type 2 interference. Because of the steeply plunging F_2 hingelines, vertical sections normal to the D_2 shortening direction show fold styles ranging from angular, open folds to circular interference shapes (Fig. 3b). Accordingly, plan views are better indicators of fold interference style and F_2 fold style.

Structures most closely resembling domes and basins characterize the model with relatively small shortening strains in both directions (c222; Figs. 3c–e). The F_2 folds with straight hinges and planar, upright axial surfaces occur in domains lacking F_1 folds (central regions of Figs. 3c–e). The 'L'- and 'T'-shaped folds occur where F_1 and F_2 folds abut but do not overprint one another (Fig. 3d) (cf. Skjernaa 1975). The F_1 and F_2 fold intersections locally form the corners of square domes or basins. Where F_1 folds were well developed, their axes and axial surfaces refolded about steeply dipping F_2 axes as open, lobate–cuspate style F_2 folds (Figs. 3d & e). Because of the spatial variation in interference style, it is locally difficult to determine the sequence of fold superposition.

Fold interference is characteristically Type 2 for models with D_1 shortening > 20%, regardless of the amount of D_2 shortening (models c213, c217, c218, c220 and c221). In plan view, F_1 hingelines and axial surfaces are refolded as broad box, chevron or lobate–cuspate style F_2 folds (Figs. 4a–c). The F_2 hinges curve gently and change plunge along their length. Minor domes and basins are locally parasitic upon larger crescent-shaped structures. The hinges of minor domes and basins and the grid lines commonly fan around the F_2 axial trace (Fig. 4c). Narrow zones of tightly refolded F_1 folds occur in conjugate sets that are oblique to both shortening directions and parallel to the axial traces of the box-style F_2 folds (Figs. 4a & c). The conjugate sets are distributed throughout the model and thus are not corner effects. The grid markers are offset with an opposite sense of shear on either set of the conjugate zones and the zones are commonly structural crests. Intersection of the conjugate strain zones and change in F_2 hinge orientation coincide with F_1 periclinal depressions. The F_1 hinges that were marked prior to D_2 do not coincide with the deformed F_1 crests, evidence of hinge migration (Fig. 4c).

Horizontal sections of models with >20% D_1 shortening show a combination of complex elliptical and crescent map patterns and a change of structural style with depth (Fig. 4b & d). Interference patterns of shallow sections show simple crescent shapes and ellipses elongate parallel to the axial traces of box-folds and minor domes. Deeper horizontal sections show F_1 axial traces refolded into chevron, cuspate–lobate and box-style folds. The PL layers tend to be faulted, fractured and boudinaged in the conjugate zone traces. Additionally, the conjugate zone intersections are loci of the most complex interference shapes. The progression from inner to outer arc of a F_2 fold is typically expressed as a

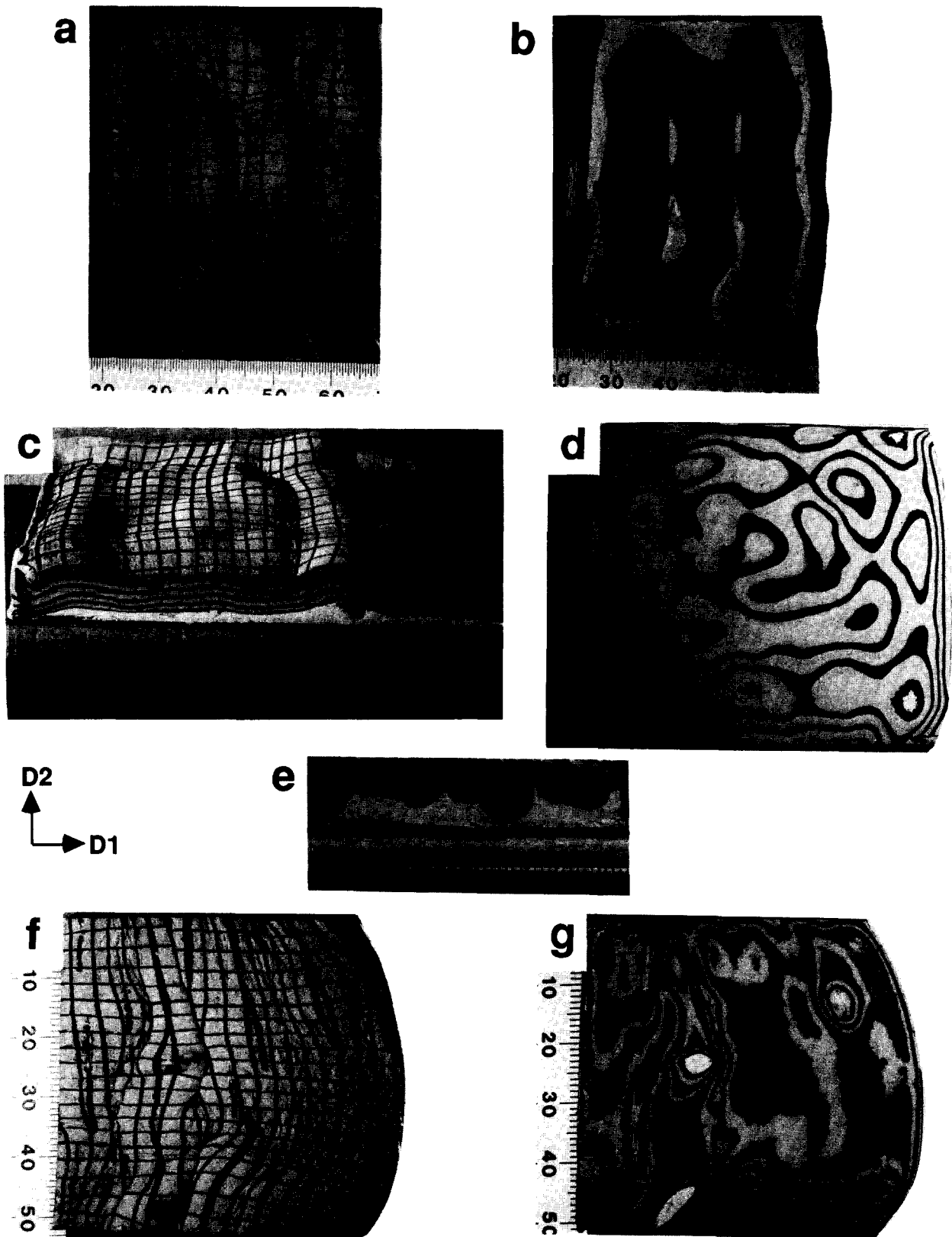Fig. 2. Models with low competence contrast layering. The strips of laminate inserted post-D_1 and pre-D_2 were cropped from most of these and subsequent photographs. For all photographs, the surface grid was initially square with 5 mm spacing, the lightest colored material is DC silicone putty and the scale bar is in mm. (a) Model c215, $D_1 = 44\%$, $D_2 = 31\%$, PL laminate, top surface. (b) Model c215, horizontal section 12 mm deep. (c) Model c216, $D_1 = 36\%$, $D_2 = 31\%$, DC–PL mixture, oblique view with profile of F_1s in the foreground. (d) Model c216, horizontal section 10 mm deep. (e) Model c224, $D_1 = 52\%$, $D_2 = 44\%$, DC–PL mixture, profiles of F_1 folds before D_2. (f) Model c224, top surface. The F_1 crests were linked prior to D_2. (g) Model c224, horizontal section 6 mm deep.
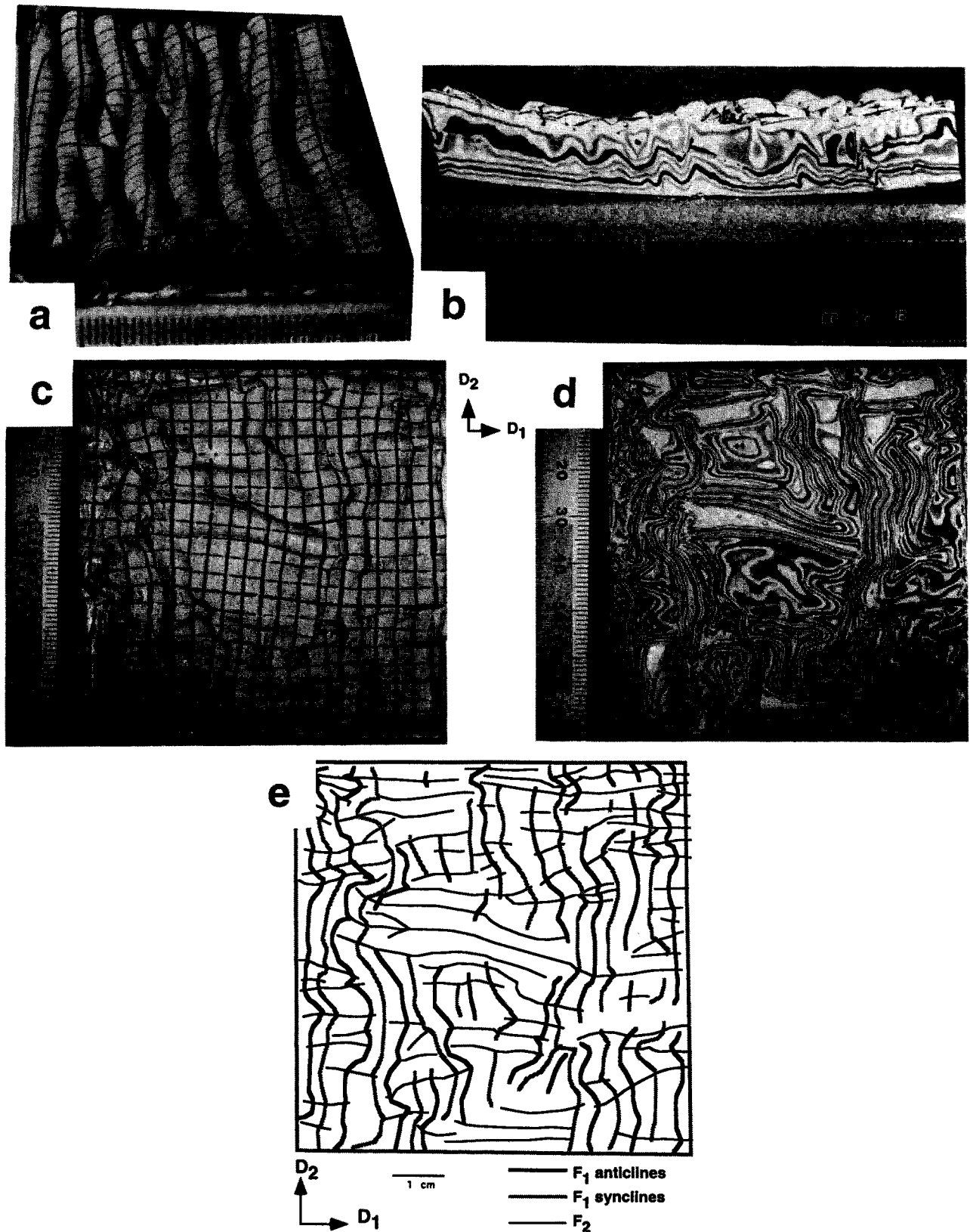
479

Fig. 3. Models with high competence contrast layering. Laminates in all models have alternating layers of DC (lightest colored layers) and PL (dark layers). (a) Oblique view of periclinal F_1 folds prior to D_2 (model c217, $D_1 = 44\%$, $D_2 = 33\%$). (b) Typical F_2 profiles (model c218, $D_1 = 54\%$, $D_2 = 20\%$). (c) Model c222, $D_1 = 17\%$, $D_2 = 18\%$, upper surface. (d) Model c222, horizontal section 10 mm deep. (e) Axial traces from c222, horizontal section 10 mm deep.
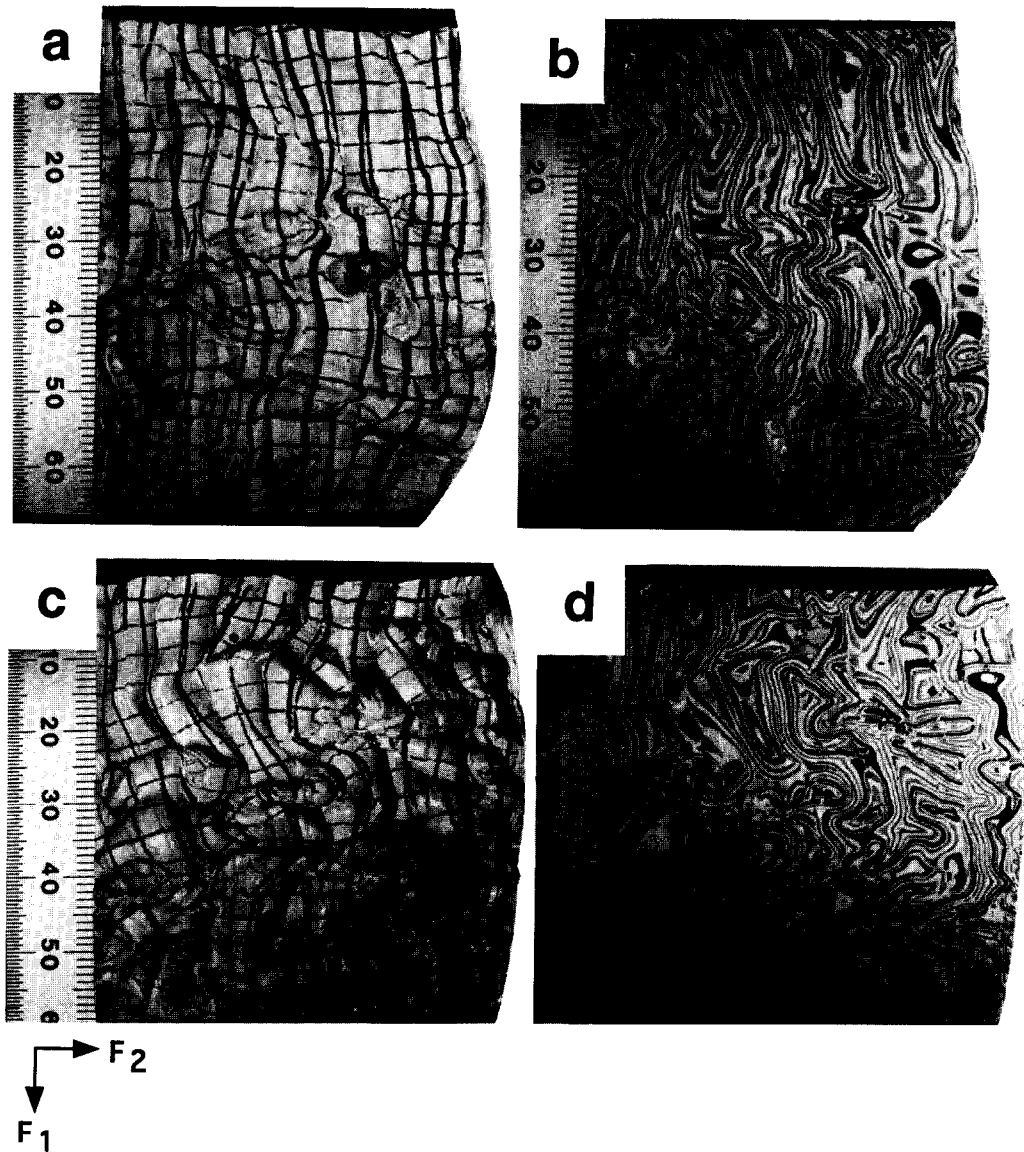
Fig. 4. Models with high competence contrast layering. (a) Model c218, $D_1 = 54\%$, $D_2 = 20\%$, upper surface. (b) Model c218, horizontal section 10 mm deep. (c) Model c217, $D_1 = 44\%$, $D_2 = 33\%$, upper surface. Hinge migration is evident in the difference between inked pre-D_2 F_1 crests and the present F_1 crests. (d) Model c217, horizontal section 14 mm deep.

Table 3. Models with low competence contrast

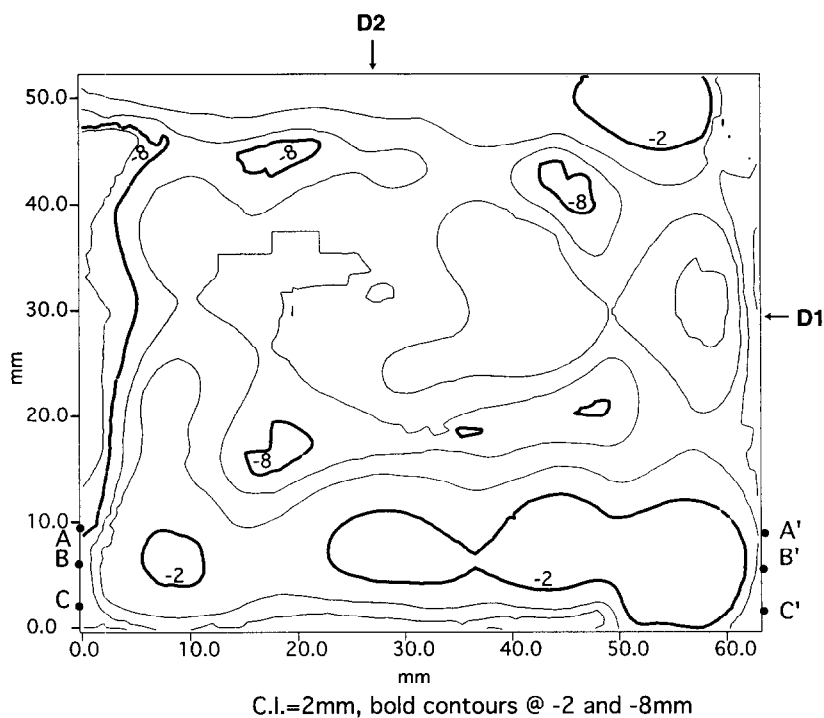| Model No.	Materials	No. of layers	% Shortening		Mean wavelength (cm)	
			D_1	D_2	F_1	F_2
c223	DC	12	34	39	N/A	N/A
c226	DC	12	65	56	N/A	N/A
c215	PL	16	44	31	1.30	2.25
c216	DC–PL mix	12	36	31	1.76	1.25
c224	DC–PL mix	12	52	44	1.03	1.70

C.I.=2mm, bold contours @ -2 and -8mm

Fig. 5. Structure contours of the top surface of c216 (compare with Fig. 2c). Transects A–A', B–B' and C–C' are the domains plotted in Fig. 6b.
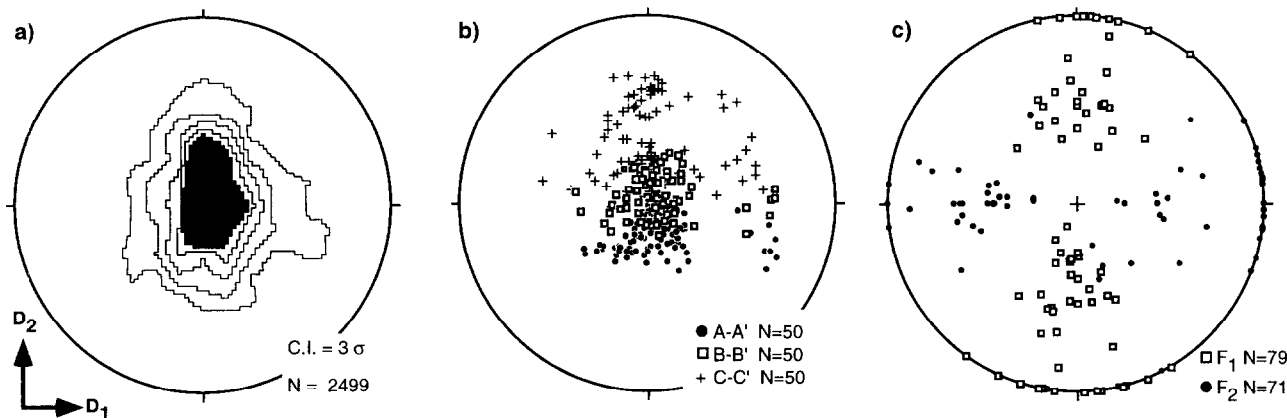
Fig. 6. (a) Equal-area projections of 2500 equally distributed poles to upper surface of the model, contoured according to Kamb (1959). (b) Equal-area projections of poles to bedding for domains A–A', B–B' and C–C' (see Fig. 5). (c) Equal-area projections of F_1 and F_2 hingelines measured directly from the structure contours.

change in interference style from ellipses elongate normal to the D_2 shortening direction, to tight crescents, to broad crescents elongate-normal to the D_1 shortening direction. Axial traces at different depths show a change from cuspate to lobate, or from single- to double-hinged (c217; Figs. 7 and 8). Note that the fold style of F_1 axial traces is similar to the style of F_1 folds in profile (compare Figs. 7 and 3a). The F_2 axial traces branch or bifurcate at different depths. Axial traces from different depths projected onto the same plane demonstrate that both F_1 and F_2 axial surfaces dip steeply (Fig. 8).

Differences between the interference styles in models with $> 20\%$ D_1 shortening are related to the amount of shortening in each direction. Increased degree of D_1

Table 4. Models with high competence contrast

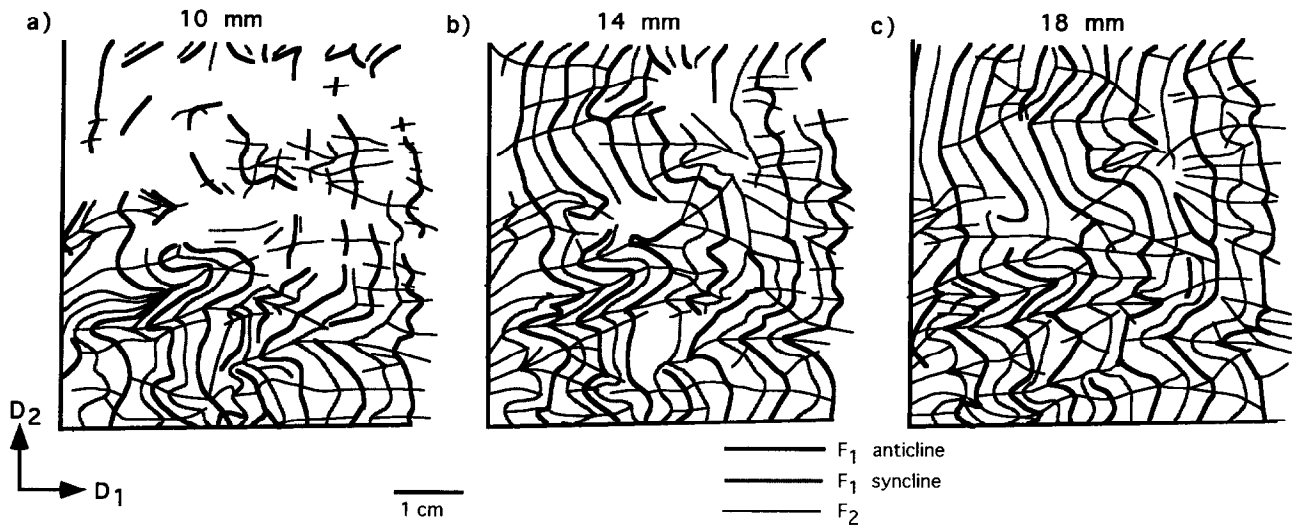| Model No.	Materials	No. of layers	% Shortening		Mean wavelength (cm)	
			D_1	D_2	F_1	F_2
c222	DC&PL	12	18	17	0.83	1.01
c218	DC&PL	12	54	20	0.64	1.30
c217	DC&PL	12	44	33	0.63	1.20
c220	DC&PL	12	37	37	0.68	1.14
c221	DC&PL	12	33	33	0.70	1.90
c213	DC&PL	16	28	38	0.61	0.69

Fig. 7. Axial traces of model c217 (compare with Fig. 4d). The F_1 axial traces are refolded into lobate–cuspate and box-style folds. The F_2 axial traces are defined by the maximum curvature of F_1 axial traces, small domes and basins superimposed upon the broader refolded F_1 axial traces and the conjugate traces of box-style F_1 axial traces. (a) 10 mm deep; (b) 14 mm deep; (c) 18 mm deep.
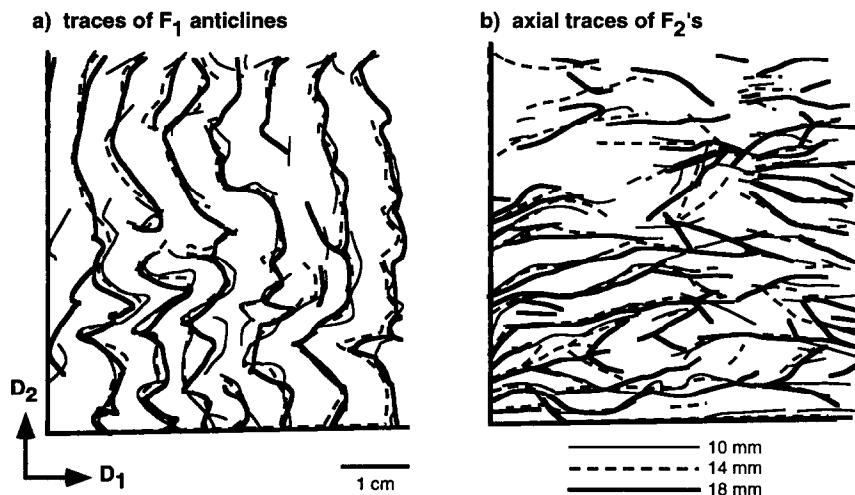
Fig. 8. Axial traces of model c217. (a) Traces of F_1 anticlines, projected onto a single plane. (b) The F_2 axial traces projected onto a single plane.

shortening relative to D_2 shortening generally correlates with the development of the conjugate strain zones. For a high ratio of D_1 to D_2 shortening, F_2 folds have a pronounced box style in plan view (c218, D_1:D_2 = 2.7; Figs. 4a & b). An approximately equal ratio of D_1 and D_2 shortening favors the development of rounded, lobate–cuspate style F_2s (c221; D_1:D_2 = 1; c220, D_1:D_2 = 1; c217, D_1:D_2 = 1.33; Figs. 4c & d). Hinge migration

is most obvious in models with approximately equal degrees of D_1 and D_2, suggesting that a minimum amount of D_1 shortening is necessary to develop the F_1 hinge, yet a high degree of D_1 shortening results in a sharp F_1 hinge zone where fold axis migration is inhibited (cf. Ghosh et al. 1993). For a low ratio of D_1 to D_2 shortening, open F_1 folds are refolded as open F_2 folds (c213; D_1:D_2 = 0.73). There, the conjugate zones
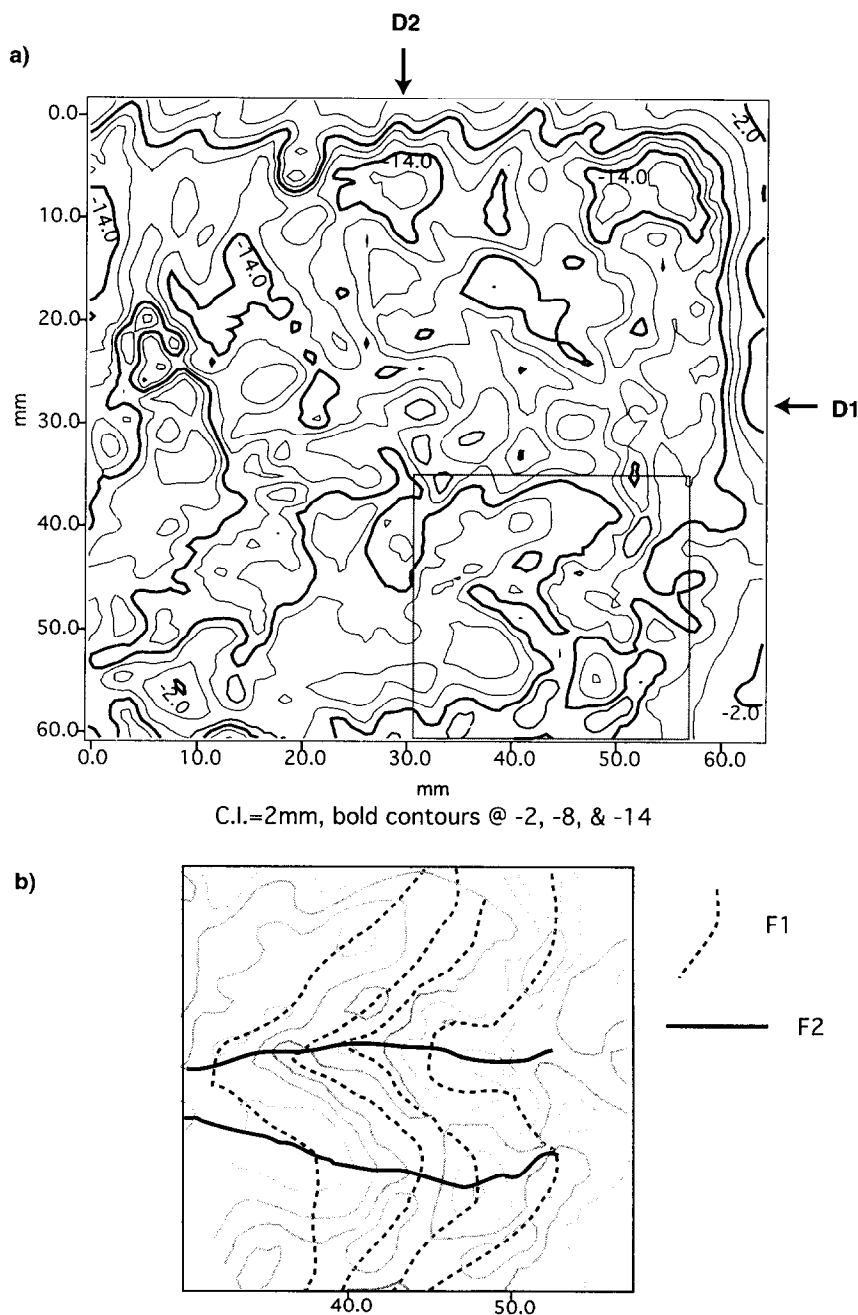
Fig. 9. (a) Structure contours of the upper PL surface of c217. (b) Enlargement of boxed area in (a). The F_1 and F_2 axial traces bound the structural domains in Fig. 10.

are weakly defined by broad, crescent-shaped map patterns or folds in the F_1 axial traces.

Structure contours of the uppermost PL surface illustrate the highly non-cylindrical fold style (c217, D_1 = 44%, D_2 = 33%) (Fig. 9). Because the structural style of refolded high competence contrast layering is more complex, this reconstruction may be less accurate than the reconstruction for the model with low competence contrast layering. No structural trend is evident from the projection of 2400 equally distributed poles to this surface (Fig. 10a, compare with Fig. 6a). The lack of vertical dips on the stereogram may be an artifact of smoothing done by the contouring software. Structural trends are most apparent if some of the data are separated into domains defined by major F_1 and F_2 axial traces (Fig. 10b).

The F_1 hinges measured from the structure contours vary in both trend and plunge, but are predominantly horizontal (Fig. 10c). Thus, the primary effect of D_2 shortening is the refolding of originally sub-horizontal F_1 hinges within the horizontal plane, about steeply plunging F_2 axes. A secondary population of F_1 hinges varies in plunge along a N–S trending girdle, indicative of a Type 1 style of refolding. The F_1 hinges generally change trend as they cross a F_2 axial trace (Fig. 10d). Within a limb of a major F_2, the plunging F_1 hinges roughly define great circles that represent the local F_1 axial surfaces. The poor definition of the great circles
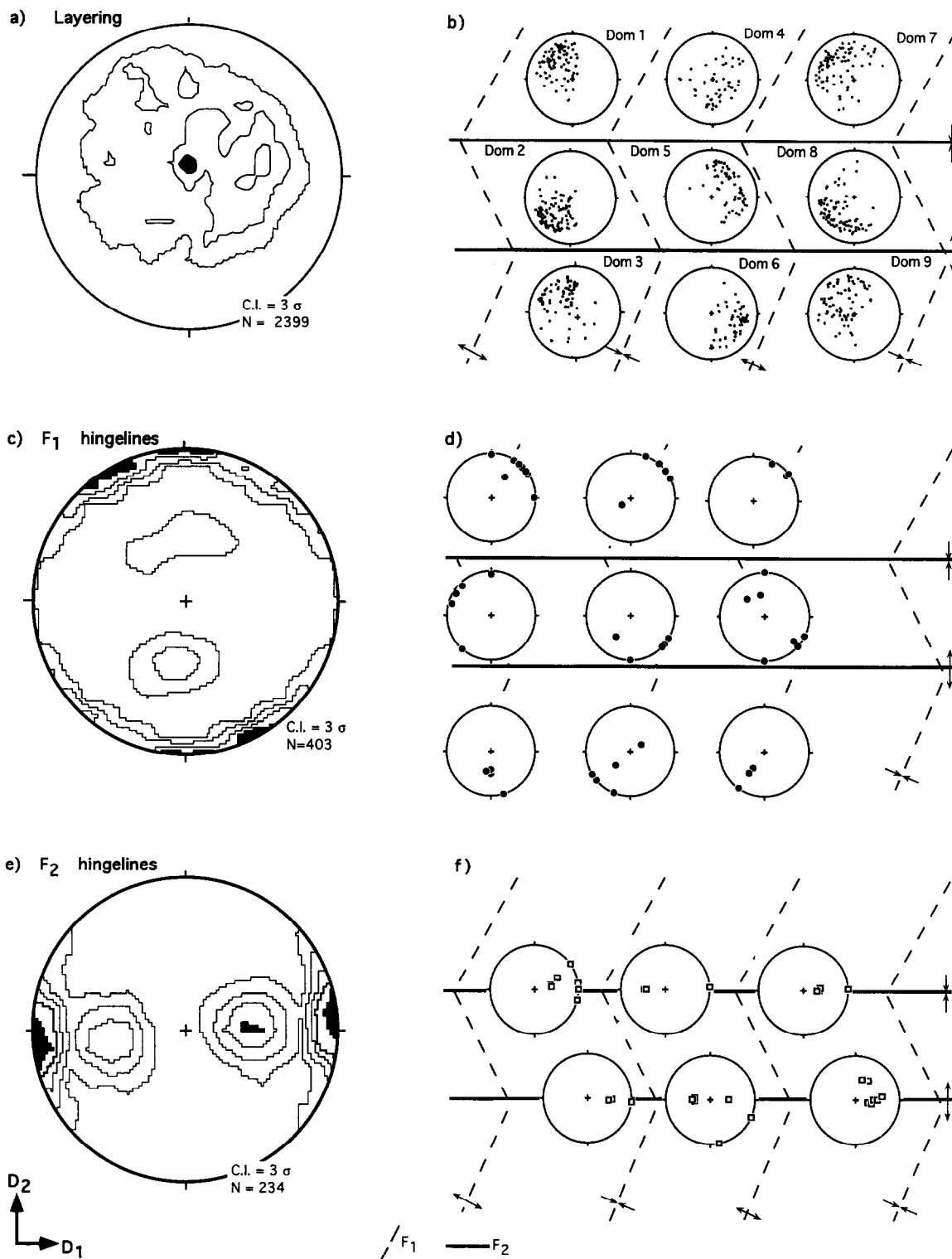
Fig. 10. Orientations of layering and fold axes for the surface contoured in Fig. 9. Fold hinge-lines were measured directly from the structure contours. Schematic axial traces illustrate the relationship between the domains and the local structures. Contoured stereograms use the method of Kamb (1959). (a) Poles to layering over entire surface. (b) Poles to layering subdivided by domains. (c) The F_1 hingelines of the entire surface. (d) The F_1 hingelines sub-divided by domain. (e) The F_2 hingelines measured from entire surface. (f) The F_2 hingelines sub-divided by domain.

suggests that even within a limb, the axial surfaces are non-planar and the fold style is non-cylindrical.

The F_2 hinges measured from the structure contours trend E or W, with variable plunge (Fig. 10e) (cf. Ramsay 1967 p. 545, figs. 10–28). One might erroneously interpret the spread of F_2 hinge orientations as evidence of a third folding event, with a shallow, N-

trending axis. Data separated into domains, however, show that F_2 hinges change orientation on opposite limbs of major F_1 folds (Fig. 10f). The spread in F_2 hingeline orientation results from the folding of F_1 limbs with different orientations and curvatures (cf. Ramsay 1967 p. 540), refolding of initially periclinal F_1 folds, fanning of minor F_2 hingelines around major F_2 folds

and the concentration of deformation along the conjugate traces of box-folds.

DISCUSSION

Comparison with previous work

The models of this series include many features present in previous models of superposed buckling, which were not designed to represent regional structures. Layering with low competence contrast tends to deform predominantly by layer-parallel shortening rather than buckling (cf. Ramberg 1964, Grujic 1993). In layering with a high competence contrast, open F_1 folds tend to form Type 1 interference (Ghosh & Ramberg 1968; Watkinson & Cobbold 1981, Odonne & Vialon 1987, Ghosh et al. 1992, 1993, Grujic 1993). Heterogeneities formed during D_1 cause a heterogeneous interference style (Ghosh & Ramberg 1968, Skjernaa 1975). Both Type 1 and Type 2 interference patterns are found in the same model (Watkinson & Cobbold 1981, Ghosh et al. 1992, 1993, Grujic 1993). The F_1 hinges migrate laterally during D_2 (Ghosh 1974, Ghosh et al. 1992, Grujic 1993). Different amplitude structures have different styles of fold interference (Ghosh et al. 1992, 1993). Additionally many of the mechanisms, or modes, of superposed buckling as defined by Ghosh et al. (1992, 1993) can be identified. In this study, there is no evidence of Mode 4, however, where F_1s are isoclinal and hinges do not migrate.

The results that are common to models with either insignificant (previous work) or significant (this study) body forces, therefore, should be qualitatively applicable to both outcrop- and regional-scale fold interference.

Gravitational effects

Some differences between this study and previous studies can be attributed to the influence of gravitational body forces on the fold style. The differences may account for differences between outcrop- and regional-scale fold interference where the initial fold enveloping surface is horizontal.

During D_1, centrifugal acceleration (analogous to gravitational acceleration in nature) opposes F_1 amplification (Fig. 1a). Gravity effectively damps the F_1 fold shapes, which have more pronounced box-style outer arcs than the first-generation folds of previous bucklefold interference models. In this manner, gravity contributes to the change with depth of the fold interference style. Gravity opposes F_2 amplification parallel to upright F_1 axial surfaces, so it aids F_2 amplification normal to F_1 axial surfaces, enhancing Type 2 interference. Because of the influence of gravitational body forces, the pronounced folding of F_1 axial surfaces might be more easily developed in regional-scale than in outcrop-scale superposed folds in nature, all other factors being equal.

Boundary effects

In the models, the fold style and orientation are affected by the presence of rigid boundaries. For example, structure contours have higher amplitudes near the boundaries (Figs. 5 and 9). The F_1 fold hingelines developed parallel to the moving rams; however, initially straight F_1 axial traces show no evidence of differential displacement due to adherence to the sidewalls. During D_2, the models extruded slightly into the strip of undeformed laminate (curved right-hand boundary of Figs. 2–4). The upper, free surface provided a rheologic interface that affected the deformation, especially of the low competence contrast models (see Appendix 3 for justification of deforming the models unconfined).

The effects of near-field, rigid boundaries are not ideal but may not be entirely artificial, given that natural structures depend on the presence and orientation of natural boundaries such as continental margins of preexisting basement structures (e.g. Braun 1993). In this study, the boundary conditions are not systematically varied, so their influence is difficult to quantify. Nonetheless, the boundary conditions are equivalent between the two model series, making the results comparable. Differences between the models are thus dominantly controlled by variables other than boundary conditions.

Strain accommodation

Unlike previous work in which F_1 fold style was the primary determinant of interference style (Ghosh & Ramberg 1968, Watkinson & Cobbold 1981, Odonne & Vialon 1987, Ghosh et al. 1992, 1993, Grujic 1993), in our study competence contrast was the important variable. Low competence contrast stratigraphy accommodates shortening by a thickening and folding of the entire multilaminate package during both shortening events, rather than by buckling of individual competent layers. The fold interference is expressed as simple, laterally homogeneous Type 1 map patterns, generally lacking curvature-accommodation folds, regardless of the ratio of D_1 to D_2 shortening or the amplitude of F_1 folds (compare Figs. 2g and 3d). High competence contrast stratigraphy accommodates shortening by buckling of the more competent PL layers and thickening of the DC silicone putty layers in the fold hinges. The interference patterns are complex hybrids between Type 1 and Type 2 interference, with Type 2 interference dominant. Both F_1 folds in profile and F_2 folds in plan view included cuspate–lobate, chevron and box-style folds, fold styles consistent with a buckling mechanism. The style of fold interference is heterogeneous laterally and with depth. The F_2 fold wavelength is generally greater than F_1 wavelength, regardless of percent shortening in either direction, suggesting that the corrugation of the model during D_1 establishes a structural anisotropy (Watkinson & Cobbold 1981) that strengthens the model (Ramsay 1967 p. 548).

The presence of a basal detachment controls the

shortening of both high and low competence contrast laminates. The rheologic contrast between the detachment and the laminate provide a localized, planar anisotropy, which buckles during D_1. Consequently, models with low competence contrast layering do not strictly represent passive folding. Shortening of the high competence-contrast layering is accommodated by the buckling of the multilaminate package, which is more competent than the basal detachment, as well as by the buckling and fracture of individual PL layers and interlaminar flow of the less competent DC layers, resulting in different orders of folding and of fold interference (cf. Ramberg 1964, Ghosh et al. 1993).

The development of a structural anisotropy subparallel to F_1 axial surfaces facilitates the development of Type 2 fold interference. High competence contrast laminates that were shortened by more than 20% deformed in a lobate–cuspate F_1 fold style, so that the DC basal detachment flowed into the cusps of the F_1 anticlines. The resultant alternation of steeply dipping laminate with the less competent detachment defined an anisotropy that is roughly parallel to F_1 axial surfaces. For example, deep horizontal sections show lobate–cuspate F_2 folds cored by DC cusps. Field examples of analogous steeply dipping detachments associated with km-wavelength refolding are described by van Berkel et al. (1984), Schwerdtner et al. (1988), and Schwerdtner & van Berkel (1991). In models with low competence contrast, and in models with high competence contrast but low D_1 shortening, Type 2 interference is rare because the D_1 anisotropy is weakly developed.

The D_1 structural anisotropy also aids the development of box-style F_2 folds and the partitioning of the D_2 shortening strain into the conjugate high-strain zones. The pronounced box-style F_2 folds in map view that characterize models with a high degree of D_1 shortening (Fig. 4a) are thus broadly analogous to kink folds that develop in profile in highly anisotropic rocks (e.g. Dewey 1965, Cobbold et al. 1971).

Although for similar folds the bulk shortening and elongation directions control the style of fold interference (Ramsay 1962, 1967 p. 521), in our study the bulk strain axes were not the chief control. Indeed, Grujic (1993) demonstrated experimentally that D_2 extension direction is a minor influence on interference type of superposed buckle folds. In our study, the bulk strain axes were not systematically varied. The D_2 direction of maximum shortening was fixed, but the D_2 extension direction may have varied. During D_2, rigid walls parallel to the F_1 axial surfaces impeded significant horizontal extension, normal to the F_1 axial surfaces. Slight extrusion into the strip of undeformed laminate inserted prior to D_2 (Figs. 2–4), however, is evidence of a component of D_2 extension normal to the F_1 axial surfaces. Thus the models' boundary conditions did not impose bulk plane strain for D_2, allowing the development of both Type 1 and Type 2 interference. Although the highly strained, low competence-contrast model extruded into the undeformed laminate strip, it lacked Type 2 interference (c224; Fig. 2g), further evidence

that rheology rather than boundary conditions controlled the interference style.

Implications for field analysis of regional fold superposition

Low competence contrast. The models predict that in rocks with low competence contrast, folds interfere as simple domes and basins. In the field, such structures would be recognized as simple map patterns without curvature-accommodation folds, with planar foliation and with a variety of plunges, but consistent trends for both F_1 and F_2 hingelines (Ramsay 1962). The sequence of folding would be ambiguous from the geometry of the structures alone.

Both Type 1 and Type 2 fold interference have been described for high-grade metamorphic rocks with a similar fold style, where little competence contrast is expected (e.g. Ramsay 1962). In such cases, the style of fold interference is more likely controlled by variables not tested in the present study, such as kinematic directions (Ramsay 1967 p. 520) or the presence of axial-planar schistosity.

High competence contrast. The models predict that superposed folds in strata with high competence contrast interfere as a complex hybrid of Type 1 and Type 2 deformation. Just as buckle folds have a more heterogeneous strain distribution than passive folds, buckle-fold superposition in the models produces a characteristically heterogeneous interference style. In the field, fold generations are differentiated on the basis of orientation, style and overprinting relationships (e.g. Ramsay 1967 pp. 520–553, Williams 1985). Because the models represent regional-scale fold superposition, the lateral and depth variation of F_1 and F_2 trends and interference style are analogous to map-scale heterogeneity. Recognition of the factors that affect the local style and orientation of structures formed by superposed buckling may help regional correlation of fold generations in rocks.

In the models where D_1 shortening is less than 20%, the initial F_1 fold distribution affects the interference style (Figs. 3c–e) (cf. Ghosh & Ramberg 1968, Skjernaa 1975). If domains of different initial F_1 style and distribution were mapped independently, the regional fold sequence might be misinterpreted and only one fold generation identified. Where the F_1 and F_2 folds abut without overprinting, the map patterns resemble Type 2 crescent shapes, and the axes of symmetry of the 'L'-shaped folds could be misinterpreted as a fold axis unrelated to either fold generation.

The initial F_1 fold orientation affects the F_2 fold style. In the models, F_1 periclinal depressions coincide with complex F_2 fold style (cf. Ghosh & Ramberg 1968 Fig. 8 p. 98, Skjernaa 1975). In the field, discontinuous F_1 or F_2 axial traces, intersection of box-fold axial traces, irregular interference patterns with multiple inflections of curvature, or a distinct, localized change in fold style of deformed F_1 axial traces could be evidence of variation
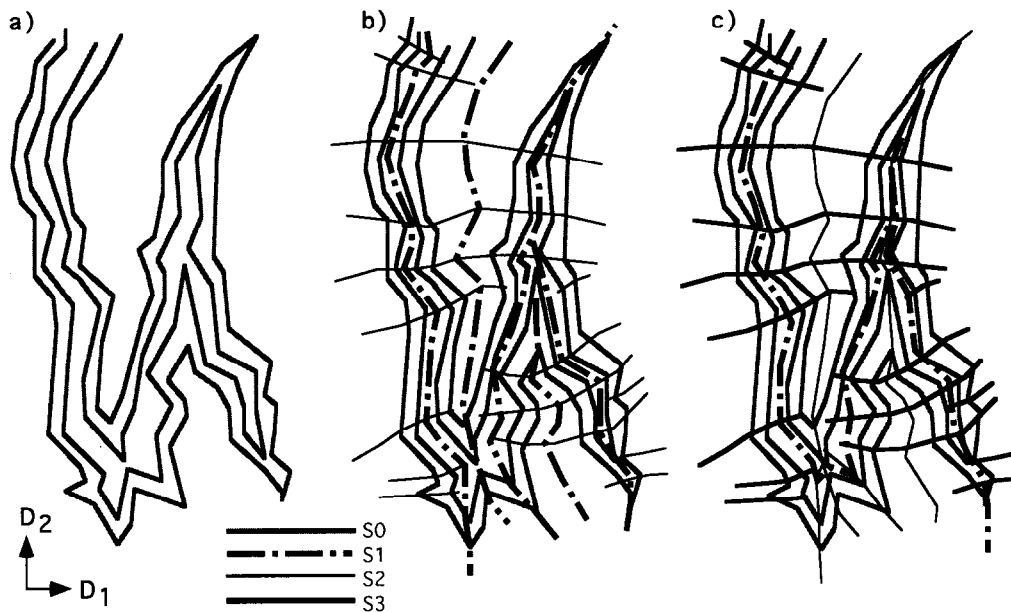
Fig. 11. An interference map pattern (part of Fig. 4b) with two interpretations that could be differentiated by foliation traces (S_1, S_2, S_3) axial planar to each fold generation. (a) Trace of layering (S_0). (b) Interpretation from known surface structure (Fig. 4a). Two phases of folding produce two distinct, nearly orthogonal, axial planar foliation traces (S_1 and S_2). (c) Foliation traces if three fold generations formed the same map pattern.

in the initial plunge of F_1 hingelines. Additionally, in some of the models adjacent or bifurcating F_1 periclines have axial traces that appear to be coaxially refolded (e.g. left, central portion of Fig. 4b). Buckling of these axial traces could be misinterpreted as a third phase of folding in the absence of cross-cutting cleavages or refolded lineations (Fig. 11).

Refolded F_1 hinges show a spread in orientation that is difficult to interpret from the stereogram alone. The equal-area projections of folded F_1 hinges form neither a great circle distribution expected for shear folding nor a small circle distribution expected for flexural-slip folding (Fig. 10c) (Weiss 1959, Ramsay 1967 p. 550). Perhaps the data do not fit either of these end-member models because the F_1 hinges do not rotate as passive lineations (cf. Ghosh 1974). Hinge migration with respect to grid markers is further evidence of non-passive behavior of early fold hinges (Ghosh 1974, Skjernaa 1975, Ghosh et al. 1993, Grujic 1993). Hinge migration could be recognized in the field as lineations, such as veins or the axes of minor crenulations, that do not coincide with the present fold hinge, or by axial-planar foliation that transects refolded F_1 hingelines (Odonne & Vialon 1987).

Steeply plunging F_2 hingelines are associated with box-style interference patterns in the models. Analogous map patterns in nature would be expressed as broad, straight-limbed regions offset by conjugate zones of high strain, or as kinks of F_1 schistosity (cf. Rixon et al. 1983, Powell 1984, Powell et al. 1985, Kano et al. 1990). Mapping within a straight-limbed domain of a box-style fold may yield no evidence of fold superposition. The conjugate zones could be erroneously mapped as shear zones or as axial traces of folds that are independent in orientation and origin of both fold generations, especially if only one of the zones were exposed. The

presence of box-style F_2 folds in plan view could be used to infer a strong anisotropy developed during D_1.

Cuspate–lobate style F_2 folds in plan view show a progressive change in interference style from inner to outer arc (e.g. model c217; Fig. 4c). Grid markers and hinges of minor folds fan around the major F_2 axis. In the field, these features correspond to fanning cleavage and radiating minor hinges (cf. variation in 'radial' fold orientation, Julivert & Marcos 1973 fig. 1). The dispersion of D_2 structural elements could be misinterpreted as evidence for additional phases of shortening. This style differs markedly from interference of similar folds where the F_2 fold morphology and orientation is spatially constant (e.g. card-deck models of O'Driscoll 1962, 1964).

The models show variation of fold style with depth. Locally, small Type 1 interference patterns, elongate-normal to the D_2 shortening direction, are superimposed on the crests of larger wavelength Type 2 patterns (Figs. 4b & d). Sections at different depths show that F_1 axial traces change fold style from cuspate to lobate or from single- to double-hinged (Figs. 7 and 8). In the field, different erosional levels may expose a change from Type 1 to Type 2 interference map patterns or different styles of refolded axial traces or schistosity. Because of such local variation in the interference style, the outcrop-scale fold style does not necessarily represent the regional-scale interference style (Watkinson & Thiessen 1988, Ghosh et al. 1993).

The complex interference style of superposed buckle folds seen in the models underscores the necessity of dividing a region into domains with constant fold styles and orientation for analyses of equal-area projections. The projection of fold axes and poles to bedding and the separation of data by domain are well-established techniques for the analysis of polydeformed regions (e.g.

Weiss 1959, Ramsay 1967 p. 551). This study predicts that data may need to be divided into smaller domains for regions of superposed buckle folds than for superposed passive folds because buckle-fold interference produces more local variation in structural style and orientation (compare domains used to construct stereograms, Figs. 5 and 9).

CONCLUSIONS

Physical models deformed under conditions of significant gravitational body forces show many of the same features as previous physical models of fold superposition, deformed under conditions of insignificant gravitational body forces. Thus the results are qualitatively comparable to both outcrop and regional-scale natural fold interference. Gravitational body forces effectively damp the vertical amplitude of both the first and second generation folds, thereby enhancing the formation of Type 2 interference.

Rheology is a significant control of fold interference style. For low competence contrast layering, fold interference is characterized by simple, homogeneous domes and basins. For high competence contrast layering, predominantly Type 2 fold interference is heterogeneous laterally and with depth. The presence of initially periclinal F_1 folds, box-style F_2 folds with conjugate zones of high strain, minor F_2 folds that fan around major F_2 traces, change in F_2 style from the inner to outer arc, and change in F_2 style with depth produce a wide variety of style and orientations of fold interference, which could be mistaken for evidence of more than two fold generations.

REFERENCES

Blay, P., Cosgrove, J. W. & Summers, J. M. 1977. An experimental investigation of the development of structures in multilayers under the influence of gravity. *J. geol. Soc. Lond.* **133**, 329–342.

Braun, J. 1993. Three-dimensional numerical modeling of compressional orogenies: thrust geometry and oblique convergence. *Geology* **21**, 153–156.

Carter, N. 1976. Steady state flow of rocks. *Rev. Geophys. & Space Phys.* **14**, 301–360.

Cobbold, P. R., Cosgrove, J. W. & Summers, J. M. 171. Development of internal structures in deformed anisotropic rocks. *Tectonophysics* **12**, 23–53.

Dewey, J. 1965. Nature and origin of kink-bands. *Tectonophysics* **1**, 459–494.

Dixon, J. & Summers, J. 1985. Recent developments in centrifuge modeling of tectonic processes; equipment, model construction techniques and rheology of model materials. *J. Struct. Geol.* **7**, 83–102.

Dubey, A. K. 1984. Superimposed buckle folding in multilayers: interference patterns and simultaneous development with transcurrent faults. *Geoscience J.* **5**, 59–72.

Dubey, A. K. & Cobbold, P. R. 1977. Noncylindrical flexural slip folds in nature and experiment. *Tectonophysics* **38**, 223–239.

Fowler, T. J. 1989. Superposed folding in the Rockley district, Lachlan Fold Belt, New South Wales. *Austr. J. Earth Sci.* **36**, 451–468.

Ghosh, S. K. 1974. Strain distribution in superposed buckling folds and the problem of reorientation of early lineations. *Tectonophysics* **21**, 249–272.

Ghosh, S. K., Mandal, N., Sengupta, S., Deb, S & Khan, D. 1992. Modes of superposed buckling in single layers controlled by initial tightness of early folds. *J. Struct. Geol.* **14**, 381–394.

Ghosh, S. K., Mandal, N., Sengupta, S., Deb, S. & Khan, D. 1993. Superposed buckling in multilayers. *J. Struct. Geol.* **15**, 95–111.

Ghosh, S. K. & Ramberg, H. 1968. Buckling experiments on intersecting fold patterns. *Tectonophysics* **5**, 89–105.

Grujic, D. 1993. The influence of initial fold geometry on Type 1 and Type 2 interference patterns: an experimental approach. *J. Struct. Geol.* **15**, 293–307.

Guterman, V. G. 1980. Model studies of gravitational gliding tectonics. *Tectonophysics* **65**, 111–126.

Hubbert, M. K. 1937. Theory of scale models as applied to the study of geologic structures. *Bull. geol. Soc. Am.* **48**, 1459–1520.

Hudleston, P. 1973. The analysis and interpretation of minor folds developed in the Moine rocks of Monar, Scotland. *Tectonophysics* **17**, 89–132.

Jackson, M. P. A., Talbot, C. J. & Cornelius, R. R. 1988. Centrifuge modeling of the effects of aggradation and progradation on syndepositional salt structures. *University of Texas at Austin Bureau of Economic Geology* R I. **173**, 93 pp.

Julivert, M. 1986. Aerial balancing and estimate of areal reduction in a thin-skinned fold and thrust belt (Cantabrian Zone, Northwest Spain). *J. Struct. Geol.* **8**, 407–414.

Julivert, M. & Marcos, A. 1973. Superimposed folding under flexural conditions in the Cantabrian Zone (Hercynian Cordillera, Northwest Spain). *Am. J. Sci.* **273**, 353–375.

Kamb, W. B. 1959. Ice petrofabric observations from Blue Glacier, Washington, in relation to theory and experiment. *J. geophys. Res.* **64**, 1891–1909.

Kano, K., Kosak, K., Murata, A. & Yanai, S. 1990. Intra-arc deformations with vertical rotation axes: the case of the pre-Middle Miocene terranes of southwest Japan. *Tectonophysics* **176**, 333–354.

Lan, L. & Hudleston, P. 1991. Finite-element models of buckle folds in non-linear materials. *Tectonophysics* **199**, 1–12.

Lisle, R. J., Styles, P. & Freeth, S. J. 1990. Fold interference structures: the influence of layer competence-contrast. *Tectonophysics* **172**, 197–200.

McClay, K. R. 1976. The rheology of Plasticine. *Tectonophysics* **33**, T7–T15.

Neurath, C. & Smith, R. B. 1982. The effect of material properties on growth rates of folding and boudinage: experiments with wax models. *J. Struct. Geol.* **4**, 215–229.

Odonne, F. & Vialon, P. 1987. Hinge migration as a mechanism of superimposed folding. *J. Struct. Geol.* **9**, 835–844.

O'Driscoll, E. S. 1962. Experimental patterns in superposed similar folding. *J. Alberta Soc. Petrol. Geol.* **10**, 145–167.

O'Driscoll, E. S. 1964. Interference patterns from inclined shear fold systems. *Bull. Can. Petrol. Geol.* **12**, 279–310.

Perrin, M., Oltra, P. & Coquillart, S. 1988. Progress in the study and modelling of similar fold interferences. *J. Struct. Geol.* **10**, 593–605.

Pfiffner, O. A. & Ramsay, J. G. 1982. Constraints on geological strain rates: arguments from finite strain states of naturally deformed rocks. *J. geophys. Res.* **87**, 311–321.

Powell, C. McA. 1984. Terminal fold-belt deformation: relationship of mid-Carboniferous megakinks in the Tasman fold belt to coeval thrusts in cratonic Australia. *Geology* **12**, 546–549.

Powell, C. McA., Cole, J. P. & Cudahy, T. J. 1985. Megakinking in the Lachlan Fold Belt, Australia. *J. Struct. Geol.* **7**, 281–300.

Raj, S. 1984. Study of interference patterns produced by fold superposition at moderate and high angles to the early fold trend in model experiments and their application to analogous structures in a lesser Himalayan terrain in Simla hills. *Geosciences J.* **5**, 25–34.

Ramberg, H. 1964. Selective buckling of composite layers with contrasted rheological properties, a theory for simultaneous formation of several orders of folds. *Tectonophysics* **1**, 307–341.

Ramberg, H. 1967. *Gravity, Deformation and the Earth's Crust; as Studied by Centrifuge Models.* Academic Press, London.

Ramberg, H. 1970. Folding of laterally compressed multilayers in the field of gravity. I. *Phys. Earth & Planet. Interiors* **2**, 203–232.

Ramberg, H. 1981. *Gravity, Deformation and the Earth's Crust.* Second edition. Academic Press, London.

Ramsay, J. G. 1962. Interference patterns produced by the superposition of folds of similar type. *J. Geol.* **60**, 466–481.

Ramsay, J. G. 1967. *The Folding and Fracturing of Rocks.* McGraw-Hill, New York.

Reynolds, D. L. & Holmes, A. 1954. The superposition of Caledonian Folds on an older fold-system in the Dalradians of Malin Head, Co. Donegal. *Geol. Mag.* **91**, 417–433.

Rixon, L. K., Bucknell, W. R. & Rickard, M. J. 1983. Megakink folds and related structures in the Upper Devonian Merrimbula Group, South Coast, N.S.W. *J. geol. Soc. Aust.* **30**, 277–293.

Schwerdtner, W. M., Torrance, J. G. & van Berkel, J. T. 1988. Pattern of apparent total strain in the bedded anhydrite cap of a folded salt wall. *Can. J. Earth Sci.* **26**, 983–992.

Schwerdtner, W. M. & van Berkel, J. T. 1991. The origin of fold abutments in the map pattern of the westernmost Grenville Province, central Ontario. *Precambrian Res.* **49**, 39–59.

Skjernaa, L. 1975. Experiments on superimposed buckle folding. *Tectonophysics* **27**, 255–270.

Smith, R. B. 1977. Formation of folds, boudinage, and mullions in non-Newtonian materials. *Bull. geol. Soc. Am.* **88**, 312–320.

Stauffer, M. R. 1988. Fold interference structures and coaptation folds. *Tectonophysics* **149**, 339–343.

Stewart, A. J. 1987. Fault reactivation and superimposed folding in a Proterozoic sandstone–volcanic sequence, Davenport Province, central Australia. *J. Struct. Geol.* **9**, 441–455.

Stewart, S. A. 1993. Fold interference structures in thrust systems. *Tectonophysics* **225**, 449–456.

Thiessen, R. 1986. Two-dimensional refold interference patterns. *J. Struct. Geol.* **8**, 563–573.

Thiessen, R. L. & Means, W. D. 1980. Classification of fold interference patterns: a re-examination. *J. Struct. Geol.* **2**, 311–326.

Turcotte, D. L. & Schubert, G. 1982. *Geodynamics: Applications of Continuum Physics to Geological Problems.* Wiley, New York.

van Berkel, J. T., Schwerdtner, W. M. & Torrance, J. G. 1984. Wall-and-basin structure: an intriguing tectonic prototype in the central Sverdrup Basin, Canadian Arctic Archipelago. *Bull. Can. Petrol. Geol.* **32**, 343–358.

Watkinson, A. J. 1981. Patterns of fold interference: influence of early fold shapes. *J. Struct. Geol.* **3**, 19–23.

Watkinson, A. J. & Cobbold, P. R. 1981. Axial directions of folds in rocks with linear/planar fabrics. *J. Struct. Geol.* **3**, 211–217.

Watkinson, A. J. & Thiessen, R. L. 1988. Geometric models of folding at Loch Monar, Scotland, using computer simulation. *Tectonophysics* **149**, 1–15.

Weijermars, R. 1986. Flow behavior and physical chemistry of bouncing putties and related polymers in view of tectonic laboratory applications. *Tectonophysics* **124**, 325–358.

Weijermars, R. & Schmeling, H. 1986. Scaling of Newtonian and non-Newtonian fluid dynamics without inertia for quantitative modelling of rock flow due to gravity (including the concept of rheological similarity). *Phys. Earth & Planet. Interiors* **43**, 316–330.

Weiss, L. E. 1959. Geometry of superposed folding. *Bull. Geol. Soc. Am.* **70**, 91–106.

Williams, P. F. 1985. Multiply deformed terrains—problems of correlation. *J. Struct. Geol.* **7**, 269–280.

APPENDIX A

Deformation in the centrifuge

Models were deformed in a 12 by 12 cm cavity in a digitally controlled centrifuge with a 21 cm radius. All models were deformed at 25°C and a maximum angular velocity of 2000 rpm, equivalent to a centrifugal acceleration 940 times normal gravitational acceleration. The time between the starting and stopping of the centrifuge rotor was clocked with a stop-watch. Because the rate of change of angular velocity is a known, reproducible function, the total time each model deformed under steady-state rotation can be computed and compared (Table 2). During deformation, the model layering was parallel to the centrifuge walls, so that the centrifugal acceleration was directed normal to the layering (Fig. 1a).

Shortening was driven by a polyethylene ram with a stainless steel base. The ram was displaced by a spreading reservoir of dense putty (ρ = 1880 kg m^{-3}), a technique based on the spreading wedge of putty shown in Dixon & Summers (1985). The shortening rate depends on

the hydraulic head of putty in the reservoir and on the angular velocity of the centrifuge. Shortening typically began before the centrifuge reached a steady-state rotation rate. The shortening rate decreased with additional time in the centrifuge, as the hydraulic head diminished. The reservoir was filled with either a dense silicone putty or a homogeneous mixture of 50% dense silicone putty and 50% PL, which spread more slowly. The centrifuge was stopped, at approximately 5 min intervals, to photograph intermediate stages of deformation and to refill the reservoir.

Superposed shortening was achieved by using two hydraulic rams (Fig. 1b). The rams had different basal curvatures to allow sliding in different directions over the curved base of the model. The model was first shortened (D_1) parallel to the centrifuge axis by a ram with a basal curvature equal to the equipotential surface. The model was then carefully extracted from the centrifuge. The model was trimmed as it rested on a curved base. The first ram was removed and a smaller, flat-based ram was positioned perpendicular to the first. In this manner, the curvature of the model is left unchanged between D_1 and D_2. Prior to the second shortening (D_2), excess space in the model cavity was filled with a strip of undeformed laminate of the same composition and thickness as the model. In some experiments, during D_2 the model extruded into this inserted laminate.

APPENDIX B

Scaling and material properties

Physical models are reasonable analogs of natural phenomena if they are geometrically, dynamically and rheologically scaled (Hubbert 1937, Ramberg 1967 pp. 2–5, 1981 p. 2, Weijermars & Schmeling 1986). A centrifuge aids dynamic scaling by increasing the ratio of centrifugal acceleration in the model to gravitational acceleration in nature (g). Accordingly, the model-to-nature ratio of gravitational body forces (σ_r) is increased:

$$\sigma_r = \rho_r g h_r, \tag{B1}$$

where ρ_r equals the density ratio and h_r equals length ratio. Because dynamic scaling requires that all significant forces are proportional. the ratio of surface resistive or tectonic force (τ_r), controlled by the model-to-nature ratios of effective viscosity (η_r) and strain rate ($\dot{\varepsilon}_r$), must also increase:

$$\tau_t = \dot{\varepsilon}_r \eta_r. \tag{B2}$$

Increased acceleration in a centrifuge therefore allows use of more viscous modeling materials than could be used in dynamically scaled models at normal gravitational acceleration. More viscous materials have the advantage of being easier to roll into fine layers, as well as being easier to cut and photograph without inducing further deformation.

Rheologic similarity requires that the model and natural materials follow a similar flow law and that the viscosity ratios between strata are equal in model and nature (Weijermars & Schmeling 1986). Dow Corning silicone bouncing putty and Plasticine modeling clay are both non-Newtonian visco-elastic fluids (McClay 1976, Dixon & Summers 1985, Weijermars 1986), a reasonable rheologic choice to represent buckling (e.g. Smith 1977, Neurath & Smith 1982, Lan & Hudleston 1991). Their viscosity ratio, dependent on the strain rate, is approximately two orders of magnitude for these experiments (Dixon & Summers 1985) (Table 1). At high strains, high strain rates and high viscosity contrasts, PL fractures and occasionally faults. Therefore, the deformation of the models is more closely analogous to folding and faulting at upper crustal levels than to the purely ductile processes of the lower crust (see Appendix C for justification of deforming the models unconfined). These materials have been used as analogs of unmetamorphosed, interbedded limestone and shale in previous models deformed in a centrifuge (Dixon & Summers 1985).

To apply the scaling equations, model parameters such as length, strain, and density are easily measured; viscosity, centrifugal acceleration and strain rate are estimated. Values for the natural parameters of viscosity, strain rate and density are also estimated. Substituting these values into equations (1) and (2) yields the model-to-nature ratio of lengths (Table 1).

The centrifugal acceleration varied throughout the experiment; thus several different values were compared for scaling purposes. The maximum acceleration, 940 times normal gravitational acceleration, is constant for all experiments (g_{max} in Tables 1 and 2). The average g

(g_{mean}) was computed using a linear approximation of the rate of centrifuge acceleration and deceleration. The mean equals the area under the acceleration vs time curve, divided by the total time (an analogous technique for computing normalized time in the centrifuge is described by Jackson *et al.* 1988). An additional value (g') was computed in a similar manner by disregarding the centrifuge deceleration period (because little deformation occurred then). For example, experiment c217 had a maximum gravitational acceleration equal to 940g, mean equal to 524g, and g' equal to 725g.

The exact strain rate is difficult to measure in the centrifuge because the ram velocity is affected by the centrifugal acceleration and by the hydraulic head of the reservoir. Much of the deformation took place during the first 2 min of centrifuge rotation, before its maximum, steady-state rotation rate. As the hydraulic head declined, ram displacement diminished during the period of steady-state rotation and was negligible during the period of deceleration. Because the centrifuge was stopped and restarted several times for photography, each model underwent several cycles of variable strain rate. The strain rates were calculated for several experiments, using the total strain and the total time in the centrifuge, the incremental strain and the period for each strain increment, or incremental strain and the period discounting the centrifuge deceleration. A value of 2×10^{-3} s^{-1} was chosen from these results as a representative strain rate to compute the scaling parameters.

The known and estimated experimental parameters yield a ratio of lengths (model to nature) of approximately 5×10^{-6} (Table 1). For example, 1 cm length in the model is analogous to about 2 km in nature. Individual layers in the microlaminate are approximately 0.025 cm thick, analogous to strata 50 m thick in nature. In summary, use of the centrifuge allows use of relatively viscous materials to represent regional-scale structures that are affected by both tectonic and gravitational forces.

APPENDIX C

Preliminary experiments

To test the necessity of a basal detachment, three models were constructed with the laminate placed directly on a rigid, lubricated base. Laminates of different colors of DC (model c223, $D_1 = 34\%$, $D_2 = 39\%$; c226 $D_1 = 65\%$, $D_2 = 56\%$) thickened rather than buckled. No surface topography developed after either the first or second deformation; however, the surficial grid strain is heterogeneous. The deformation is associated with perturbations around air bubbles, in both profile and map view. No periodic structures resembling folds formed. Layer-parallel shortening is approximately 200% for model c223 and 500% for model c226. For high competence contrast layering without a detachment, tight chevron folds formed preferentially at the boundaries of the model, adjacent to the moving ram and the opposite wall. Few folds developed in the center of the model, away from the boundaries. A thick detachment was used to help distribute the deformation away from the model boundaries.

Fold theory predicts that the dominant fold wavelength increases for a viscous system with inverted density stratification under the influence of gravity (Ramberg 1970). Dow Corning silicone putty has a lower density than Plasticine or the PL–DC mixture ($\rho = 1450$ kg m^{-3}). To test whether the folding was affected by the buoyancy of the basal CD layer, one model was constructed with a dense basal detachment ($\rho = 1800$ kg m^{-3}), made of a mixture of powdered galena with Rhodorsil gomme, a silicone bouncing putty. Folds were found to have the same style and mean wavelength as models with the less dense DC detachment. Apparently, under these experimental conditions, buckling is more strongly controlled by the viscosity contrast of the laminate than by the density of the matrix. Because it was more readily available, DC was used as the detachment material.

To test whether the laminate needed its upper surface confined, two models were constructed with different confining materials. A 3 mm layer of PL was used as the strong confining layer above a 3 mm bilaminate with a 1 mm DC basal detachment. When shortened 30% in one direction, the PL buckled with an average wavelength of approximately 17 mm, more than twice the wavelength of the unconfined bilaminate. In the inner arc of the PL folds, the laminate deformed as short wavelength, tight folds. In the outer arc, the laminate folded with the same wavelength as the PL confining unit. Although this stratigraphy may represent some geologic occurrences, this study seeks to model the multilayer folding without the influence of adjacent, strong units. When a 3 mm layer of DC was tested as a weak confining layer, the DC supported no surface topography and thickened uniformly. Vertical slices through the model revealed concentric fold profiles in the bilaminate, insignificantly different in style, wavelength or amplitude from the unconfined models. The scaling parameters calculated above (Appendix B) suggest that the laminates represent a section of unconfined crust less than 1 km thick. At such shallow depths, dominantly brittle deformation is expected, but not observed in the models. Accordingly, the models are better analogs for depths where ductile processes dominate than for thrust belt structures. Because confinement of the models insignificantly affected their structural style, and to allow observation of the evolution of the top surface, the laminates were deformed unconfined.